International Journal of Engineering and Technology Innovation, vol. 15, no. 4, 2025, pp. 456-475

Factors Affecting the Mechanical Properties of Precast Concrete Infill Walls

Li-Xuan Ren*

Shandong Transport Vocational College, Weifang, China

Received 18 June 2025; received in revised form 19 August 2025; accepted 22 September 2025

DOI: https://doi.org/10.46604/ijeti.2025.15418

Abstract

Precast concrete infill walls are widely applied to enhance the lateral stiffness and seismic performance of reinforced concrete frames. This study aims to establish a quantitative understanding of how key design parameters influence the mechanical behavior of precast concrete infill wall systems. To achieve this objective, nonlinear finite element analyses validated against ATENA-based experimental results were conducted to examine the effects of wall aspect ratio, thickness, and tie reinforcement configuration on system-level stiffness, strength, and ductility. Results show that decreasing the aspect ratio from 0.67 to 0.47 increases lateral stiffness by approximately 15-20% but reduces ductility by about 10%. Increasing wall thickness from 100 mm to 200 mm enhances peak load capacity by up to 30% while shifting damage from the infill wall to the frame. Denser wall-column ties improve residual load capacity by 18-25%, whereas wider wall–beam tie spacing slightly reduces ductility without significantly affecting peak load.

Keywords: precast concrete, infill wall, finite element analysis, influence factor

1. Introduction

Currently, the application of cast-in-place concrete faces several challenges, including labor shortages, limited natural resources, and environmental concerns. Compared to traditional cast-in-place concrete structures, precast systems have been widely adopted in many buildings due to their advantages, including reduced labor requirements, improved quality control, cost-effectiveness, and ease of construction [1-2].

With China's continued economic growth and the accelerating pace of industrialization and digitalization, future building products are expected to transition toward higher quality, lower pollution, and enhanced sustainability. Conventional construction methods are increasingly unable to meet the evolving demands of the industry, making industrialization a crucial direction for future development.

Cast-in-place systems present significant limitations in achieving full building industrialization, whereas precast construction divides buildings into standardized components (columns, walls, beams, slabs, and stairs) that are manufactured in factories. These components are then assembled on-site through necessary connections and partially cast-in-place joints to form a complete prefabricated structure. This approach enables the transformation of construction from traditional on-site building to factory-based manufacturing, providing an effective means for achieving building industrialization [3-5].

* Corresponding author. E-mail address: sdjtzyxyrlx@163.com

Recent statistics indicate that in China, the share of prefabricated (including precast) buildings in new construction has exceeded about 20% by 2022, with government targets aiming to raise this proportion to roughly 30% by 2030; internationally, several European countries and North American markets report precast adoption levels on the order of 30–50% depending on building type. These figures underscore both the timeliness and practical relevance of research on precast concrete systems.

In practice, conventional cast-in-place delivery in China often faces schedule delays due to on-site concreting and curing windows, weather-sensitive pours that trigger rework, and congestion from simultaneous trades. Quality consistency (QC) can also be difficult to guarantee at scale, with risks of honeycombing, segregation, uneven compaction, and dimensional tolerance drift under field conditions. Moreover, high labor demand and safety exposure, extensive formwork and temporary works along with the associated waste, and variable on-site QC further challenge cost and predictability.

Among various prefabricated components, precast concrete infill walls have attracted significant attention due to their ability to substantially improve construction efficiency, structural performance, and energy efficiency in buildings [6]. Against this backdrop, precast infill walls provide factory-controlled quality and shorten critical-path activities on site, thereby directly addressing the above schedule, quality, and labor constraints.

Research on the seismic performance of precast concrete infill walls has increased rapidly, with most studies focusing on the design of connection joints, energy dissipation mechanisms, and the integration of numerical simulation with experimental analysis. Innovations in joint configurations and performance are considered crucial for enhancing seismic resilience.

For example, Xiong et al. [7] investigated low- to mid-rise precast wall systems and demonstrated that incorporating ultra-high-performance concrete (UHPC) reinforcement at bolted connections can significantly improve the lateral load capacity and hysteretic energy dissipation of the structure. Their experimental results showed that this type of connection can achieve performance comparable to that of cast-in-place walls [8-9].

In addition, Tang et al. [10] conducted parametric analyses of precast braced shear walls, verifying the influence of wall height, axial force, and joint configuration on the structure’s hysteretic behavior and ductility. Their findings suggested about a 15% improvement in ductility under optimized joint detailing.

Furthermore, the application of double-sided steel plates or bolted steel-plate connections in lightweight sandwich wall panels has shown remarkable results. In 2024, Wang et al. [9] conducted shaking table tests on a full-scale lightweight precast shear wall model using a bolted steel-plate connection. They reported that this type of connection preserved nearly 90% of the peak load capacity after repeated cyclic loading, while enhancing ductility. The results indicated that this type of connection not only enhanced the ductility of the structure but also maintained high load-bearing capacity, offering both economic and construction advantages [7, 9]. Related studies have also found that dividing the wall into two subassemblies (a double-panel system) can yield superior hysteretic performance and energy absorption under cyclic loading compared to a single integrated wall [11-14].

Numerous studies in numerical analysis have employed finite element models to investigate the behavior of precast infilled wall structures. Zheng et al. [15] proposed a system consisting of energy-dissipating precast reinforced concrete (ED-PRC) components, incorporating a conical steel damper at the top of the precast wall to create a staged yielding mechanism involving the damper, wall, and frame. Nonlinear analysis results showed enhanced ductility and reduced frame damage. Additionally, Li et al. [16] demonstrated that using hysteretic-recoverable joints and self-recovering walls can simultaneously improve both the seismic performance and repairability of precast self-centering concrete frame systems. Overall, the literature suggests that rational joint design, effective energy dissipation strategies, and the use of UHPC or other high-performance materials enable precast infill wall structures to achieve or exceed the seismic performance of traditional cast-in-place systems.

Nevertheless, despite this progress, a systematic understanding of the influence of key design parameters on the overall performance of precast concrete infill wall systems is still lacking. Specifically, there is no unified analytical framework that quantitatively evaluates how critical factors, such as infill wall aspect ratio, wall thickness, and tie reinforcement configurations affect stiffness, load-bearing capacity, and ductility at the system level.

Moreover, although finite element methods have been widely applied, limited attention has been given to uncertainty quantification and error analysis, which are increasingly recognized as necessary to ensure robust and reliable modeling results. To address this research gap, nonlinear finite element analyses were conducted and validated against experimental benchmarks. These analyses systematically investigate the effects of aspect ratio, wall thickness, and tie reinforcement arrangements on the mechanical properties of precast concrete infill wall systems.

Specifically, the professional concrete analysis software ATENA is employed, which is recognized for its accuracy in simulating the behavior of concrete cracking, crushing, and reinforcement. The primary objectives of this study are: (1) to validate the finite element model against experimental data, ensuring credible simulation; (2) to conduct a parametric analysis that quantitatively assesses the influence of geometry and reinforcement detailing on stiffness, strength, and ductility; and (3) to provide practical recommendations for optimizing precast infill wall design.

The outcomes of this research will provide valuable insights to engineers and designers, facilitating more informed decisions in precast structural design and promoting the broader adoption of industrialized construction practices. In contrast to recent studies that primarily emphasize connection detailing or single-factor variations, this work provides an experiment-calibrated finite-element investigation that jointly quantifies the effects of wall aspect ratio, wall thickness, and both wall–column and wall–beam tie configurations on system-level stiffness, strength, ductility, and post-peak residual capacity. This multi-factor, system-level perspective clarifies trade-offs among design choices and complements connection-focused literature.

2. Numerical modeling

The material constitutive relations described in the previous section establish the fundamental basis for simulating the nonlinear behavior of concrete and steel. Building upon these definitions, the next stage involves developing a detailed finite element model capable of reproducing the structural response of precast concrete infill walls under lateral loading. This process includes defining boundary conditions, meshing strategies, interface contact behavior, and loading procedures. The following section presents the overall numerical modeling framework adopted in this study, ensuring that the simulation accurately reflects the mechanical characteristics of the experimental specimens and provides a reliable platform for subsequent parametric analyses.

2.1. Material constitutive relation

To accurately simulate the nonlinear mechanical response of precast concrete infill wall systems, it is essential to define appropriate material constitutive relationships for both concrete and reinforcing steel. The constitutive models describe how materials behave under different stress and strain conditions, forming the foundation of finite element analysis. In this study, concrete is modeled using a fracture-plastic constitutive law capable of representing cracking, crushing, and post-peak softening, while reinforcement steel is represented by an elastic-perfectly plastic model. The following subsections outline these material models in detail, providing the necessary parameters and theoretical basis for the subsequent numerical analysis.

2.1.1. Constitutive relation of concrete

To clarify the methodology, the overall research workflow is briefly summarized here. The study was conducted in several logical stages: (i) identifying the problem and reviewing relevant literature on precast concrete infill walls; (ii) developing a nonlinear finite element model in ATENA; (iii) calibrating and validating the model against benchmark experimental data; (iv) performing parametric analyses to investigate the effects of key variables, such as aspect ratio, wall thickness, and tie reinforcement configurations on mechanical performance; and (v) interpreting the results and formulating design-oriented recommendations. This structured process ensures methodological transparency and systematic evaluation of the influencing parameters.

Concrete is an inherently complex, nonlinear material, making the simulation of reinforced concrete (RC) structures under load particularly challenging. To address this challenge, ATENA offers a comprehensive library of material models that support experimental research and enable accurate prediction of structural component behavior.

The fracture-plastic constitutive model adopted for concrete in this study is schematically illustrated in Fig. 1. It should be noted that although the overall finite element analysis in this study is conducted under a two-dimensional plane-stress framework, the constitutive relations of concrete are expressed in one-dimensional form to represent the fundamental uniaxial stress–strain response.

ATENA internally extends these one-dimensional laws to multiaxial states through tensor transformation and failure surface integration. This approach is widely accepted in nonlinear concrete modeling because the uniaxial formulation provides a clear physical interpretation and stable numerical implementation while ensuring accurate representation of cracking and crushing behavior in two-dimensional simulations.

In Fig. 1, the main parameters governing the concrete constitutive model are defined as follows: μ is the Poisson's ratio of concrete, representing the ratio between lateral and axial strains under uniaxial loading; ε_t is the tensile strain at cracking, corresponding to the strain level at which microcracks initiate and the tensile stress begins to decrease; ε_c denotes the strain at peak compressive stress, beyond which the concrete enters the softening regime; ε_d is the strain defining the descending (softening) branch of the compressive stress–strain curve, characterizing post-peak deformation capacity.

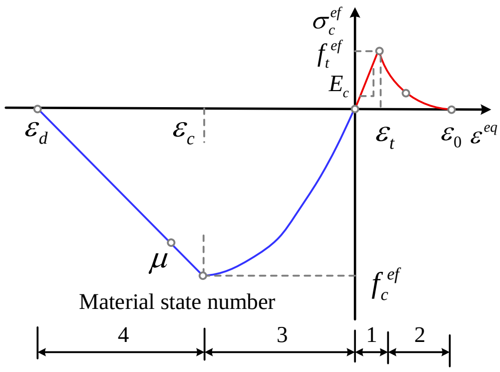

Fig. 1 Concrete Constitutive Model

Before cracking occurs, the relationship between the concrete's equivalent axial strain ε^{eq} and its effective stress σ_c^{ef} can be expressed as follows:

$$\varepsilon^{eq} = \frac{\sigma_c^{ef}}{E_c} \qquad 0 \le \sigma_c^{ef} \le f_t^{ef} \tag{1}$$

where E_c is the initial elastic modulus of concrete, and f_t^{ef} is the tensile strength of concrete, for ordinary concrete, ATENA primarily uses the softening model proposed by Hordijk (1991) [17]. The formula for this model is given as follows:

$$\frac{\sigma_c^{ef}}{f_t^{ef}} = \left[1 + (c_1 \frac{w}{w_c})^3\right] \exp(-c_2 \frac{w}{w_c}) - \frac{w}{w_c}(1 + c_1^3)\exp(-c_2) \tag{2}$$

where w is the crack width, $w_c = 5.14G_f / f_t^{ef}$ is the crack width at which the tensile stress is fully released (i.e., drops to zero); G_f is the concrete's fracture energy; and c_1 and c_2 are dimensionless shape parameters (with c_1=3 and c_2=6.93). For concrete in compression (before reaching peak stress), ATENA uses the constitutive formula recommended by the CEB-FIP Model Code 1990 [18]:

$$\begin{aligned} \sigma_c^{ef} &= f_c^{ef}\frac{kx - x^2}{1+(k-2)x} \\ x &= \frac{\varepsilon^{eq}}{\varepsilon_c} \\ k &= \frac{E_0}{E_c} \\ E_c &= \frac{f_c^{ef}}{\varepsilon_c} \end{aligned} \tag{3}$$

where f_c^{ef} is the adequate compressive strength of concrete; x is a dimensionless strain parameter (the ratio of the current strain to the strain at peak stress); k is the shape parameter; E_0 is the initial elastic modulus of concrete; and E_c is the secant modulus at peak compressive stress.

The plastic displacement w_d defines the post-peak shape of the concrete's compressive stress-strain curve. This parameter characterizes the softening branch beyond the peak load, and the fracture energy associated with creating a unit area of crack surface is implicitly determined by w_d. According to Van Mie's test results [19], a typical value for the plastic displacement in ordinary concrete is approximately 0.5 mm (i.e., w_d = 0.5 mm). The descending branch slope of the stress-strain curve in the stress-strain curve, denoted as ε_d, represents the strain increment that defines the slope of the softening branch and is governed by both the peak point and the ultimate compressive strain, providing valuable insights into the material's behavior under compressive loading. Analysis of this descending branch offers critical information for designing more robust concrete structures. The following formula gives the relationship:

$$\varepsilon_d = \varepsilon_c + \frac{w_d}{L_d} \tag{4}$$

where L_d is the area of the shear zone.

2.1.2 Structural relation of steel

Steel can be considered a nearly ideal homogeneous material. In this paper, a simplified bilinear elastic-perfectly plastic model is employed to simulate the behavior of the steel reinforcement. The resulting stress-strain relationship is as follows:

$$\sigma_s = \begin{cases} E_s\varepsilon_s, & \varepsilon_s \le \varepsilon_y \\ f_y, & \varepsilon_y \ge \varepsilon_s \end{cases} \tag{5}$$

where σ_s is the stress of reinforcement, E_s is the elastic modulus of support, ε_s is the steel strain, ε_y is the yield strain of the reinforcement, and f_y is the steel bar tensile strength.

2.2. Contact type

In ATENA, a contact surface model is used to simulate the interaction between different structural components. The interface behavior is characterized by the Mohr-Coulomb failure criterion [20]. Under compressive loading, the interface's shear capacity is governed by both its cohesive strength, c, and frictional resistance. The following formula expresses this relationship:

$$\tau = c - \mu\sigma(\sigma \leq 0) \tag{6}$$

Generally, the shear strength τ of a concrete interface depends on both its cohesive bond strength, c, and its tensile bond strength f_t. In the present study, however, the interface's shear resistance is assumed to derive primarily from friction between the concrete surfaces and the dowel action of the steel reinforcement, since any direct tensile bonding at the interface is neglected. It should be noted that within the ATENA modeling framework, the reinforcement is represented by truss elements, which do not directly capture the shear contribution of the dowel action.

For an interface under compression, shear strength is governed by both cohesion and friction according to the Mohr-Coulomb criterion, as shown in Eq. (6). The cohesive strength component, c, is determined using Eq. (7). Because the tensile bond strength of the concrete at the interface, f_t, is neglected in this study, the interface's shear capacity primarily comes from the reinforcement (through dowel action). Consequently, Eq. (7) is employed to represent the interface shear strength in the analysis:

$$c = \tau_s = \mu\gamma\rho_{sv} f_y \tag{7}$$

where c is the cohesive strength, f_y is the yield strength of the reinforcement, and γ is a coefficient representing the dowel (pinning) effect of the steel bars. The value of γ depends on the interface roughness: for a very rough interface (approximately 1.8 mm surface asperity height), γ will be relatively large, whereas for a smooth interface (~0.5 mm roughness), γ is small. In this study, an intermediate roughness of approximately 1.3 mm is assumed. Furthermore, ρ_{sv} denotes the interface reinforcement ratio, and μ is the interface friction coefficient.

3. Validation of the finite element model

To ensure the reliability and applicability of the developed numerical model, a rigorous validation process was conducted before performing parametric analyses. Model validation is a crucial step in finite element studies, as it verifies the accuracy of the adopted material models, boundary conditions, and contact representations. In this research, the numerical simulation results were compared with benchmark experimental data reported in the literature to confirm the model's ability to reproduce key structural responses, including stiffness evolution, crack patterns, and ultimate load capacity. The following subsection provides a detailed description of the experimental program and its relevance to the validation of the finite element model.

3.1. Experimental Introduction

Moretti et al. [21] conducted quasi-static tests on seven one-third-scale reinforced concrete frame-infill wall assemblies to investigate the influence of various parameters, including the infill wall aspect ratio, tensile reinforcement configuration, anchorage length, and type of frame columns, on structural performance. The experimental outcomes provide essential insights for practical design and construction. In these tests, concrete infill walls were cast after the frame had fully cured, and they were connected using pre-installed tie bars. The specimens were loaded at the beam-column joints using a ±500 kN hydraulic actuator. Initially, the loading was force-controlled in increments of 20 kN per stage. After three phases, the loading protocol switched to displacement control, progressing in increments of 0.15 mm until the specimen's load-carrying capacity was reached. The test setup is illustrated in Fig. 2.

Moretti et al. validated the finite element model by analyzing the influence of wall aspect ratio and tie reinforcement configurations on the frame response. For numerical verification in the current study, three representative specimens (A1, A2, and B1) with variations in aspect ratio and tie reinforcement arrangements were selected. Their geometric dimensions and configurations are detailed in Table 1.

Fig. 2 Experimental test setup (Adopted from [21])

Table 1 Geometric and reinforcement parameters of selected specimens (Unit: mm)

Specimen	Column size	Beam size	Wall thickness	High wall	Wall width
A1	100×100	100×100	50	750	1300
A2	100×100	100×100	50	750	1300
B1	100×100	100×100	30	750	900

Remark: Specimen A1 features both wall-beam and wall-column tie reinforcements. Specimen A2 includes only wall-beam tie reinforcement. Specimen B1 also consists of both tie types.

All specimens utilized a double-layer, bi-directional reinforcement mesh with 5 mm diameter bars in the infill walls, accompanied by consistent frame reinforcement, as shown in Fig. 3. Reinforcement yield strengths were measured as follows: 350 MPa for longitudinal frame bars, 560 MPa for stirrups, 470 MPa for tie bars, and the concrete was grade C30.

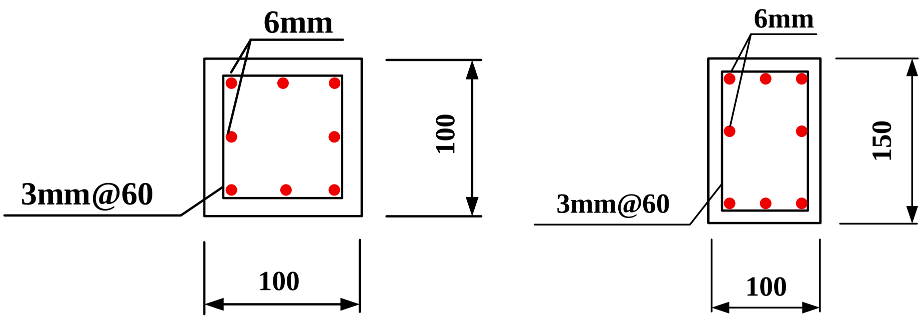

(a) Frame Column (b) Frame beam

Fig. 3 Reinforcement detailing of test specimen (Unit: mm)

3.2. Establishment of the Finite Element Model

The ATENA software was used to develop a comprehensive finite element model that replicates Moretti's experimental tests, thereby validating the numerical modeling approach and material constitutive laws. Previously defined constitutive models were used to represent the behavior of concrete, and the reinforcement was modeled using truss elements. For computational efficiency, tensile strength at the interfaces between new and existing concrete was neglected.

Loading was applied at the midpoint of a 50 mm thick mat placed at the beam's left end, with an elastic modulus of 2.0×10^5 N/mm². The height of the foundation beam was set at 300 mm, with the same modulus value. The bottom surface of the foundation beam was fully constrained. The mesh size was uniformly set at 50 mm. A schematic of the finite element model is presented in Fig. 4. Displacement-controlled loading was applied incrementally at a rate of 0.1 mm per step. Specimens A2 and B1 were loaded until they reached 85% of their respective peak loads, whereas specimen A1 experienced brittle failure at ultimate displacement.

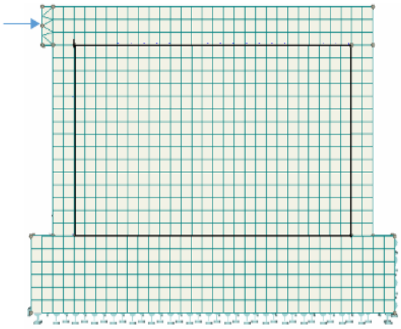

Fig. 4 Schematic representation of the finite element model

The FE model adopts idealized boundary conditions, a bilinear elastic-perfectly plastic steel model, and interface behavior represented by a Mohr–Coulomb law with friction and a dowel-action surrogate. These choices follow common ATENA practice for RC infill systems and enable stable calibration against the benchmark tests. Idealized supports may slightly over-constrain lateral drift; bilinear steel without explicit bond–slip can over-estimate initial stiffness yet capture peak strength adequately; and the adopted interface law may under-represent local slip while reproducing global load–displacement and crack patterns. The observed experiment-to-simulation discrepancies (generally < 15%) delimit the applicability of the model within the studied parameter space.

3.3. Finite Element Model Calibration Results

Fig. 5 (a) presents the observed damage locations and final crack distribution for specimen A1 based on the experimental results. It was found that the majority of the damage in specimen A1 was concentrated in the frame columns, and its ultimate failure was attributed to shear damage at the frame nodes, primarily caused by the relatively small cross-sectional dimensions of the columns. Fig. 5 (b) displays the corresponding crack pattern in the finite element simulation for specimen A1, which similarly shows pronounced cracking at the frame nodes in the final state. The simulated results closely match the experimental observations.

However, it should be noted that in the finite element results shown in Fig. 5 (b), additional fine cracks appear near the upper-right corner of the infill wall, which are not clearly visible in the experimental image shown in Fig. 5 (a). This discrepancy is attributed to localized tensile stress concentration at the beam–column interface caused by mesh discretization and idealized boundary conditions in the numerical model. Despite this local difference, the global cracking trend, primary shear-failure pattern, and final failure mode remain consistent between the simulation and experiment, confirming the reliability of the model.

Fig. 6 illustrates the damage locations and final crack distribution for specimen B1. In this case, the experimental results indicate that the base of the frame column underwent severe flexural deformation, with comparatively wider cracks forming at the base of the column.

(a) Test results (Adopted from [21]) (b) Finite element results

Fig. 5 Fracture comparison results of specimen A1

(a) Test results (Adopted from [21])

(b) Finite element results

Fig. 6 Fracture comparison results of specimen B1

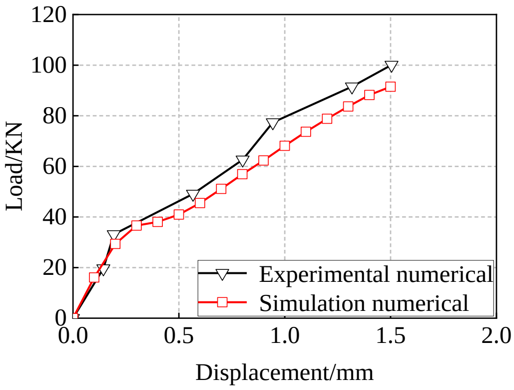

(a) Specimen A1

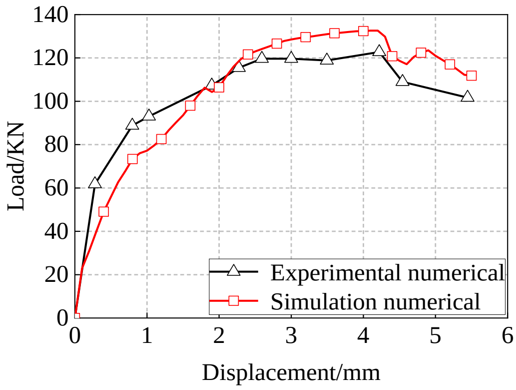

(b) Specimen A2

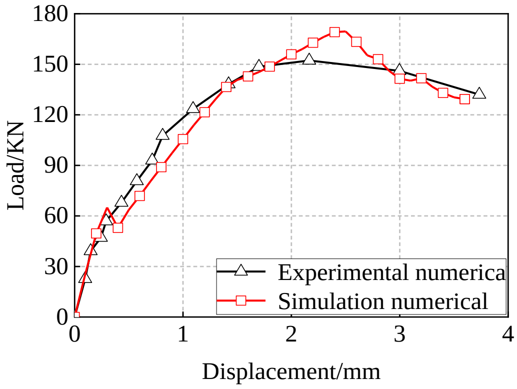

(c) Specimen B1

Fig. 7 Calibration model load-displacement curve

In contrast, the finite element model of specimen B1 in its final state exhibits cracks at the top and base of the column, as well as within the infill wall. Notably, the widest cracks are observed at the column base, which present as flexural cracks. Additional tensile cracking is evident at the wall corners, which is in good agreement with the experimental damage patterns. As shown in Fig. 7, the load–displacement curves of the concrete frame–infill wall structure simulated using ATENA closely match the experimental results, with the simulation error maintained below 15%. This agreement verifies that the developed finite element model can accurately reproduce both the stiffness evolution and ultimate load behavior observed in the physical tests, confirming its reliability for subsequent parametric analyses.

The foregoing analysis demonstrates that ATENA software effectively captures the trends in stiffness variation for concrete infill wall structures with different height-to-width ratios. However, certain discrepancies between simulation and experimental results are attributable to factors not accounted for in the modeling process, such as differences between the actual boundary conditions in the physical tests and the idealized constraints used in the finite element analysis. Additionally, the simulation does not account for the bond-slip behavior between concrete and reinforcement, which introduces some deviation between the simulated and measured responses. Nevertheless, the overall arrangement of tie reinforcement and the representation of the contact surfaces in the model are reasonable, and the simulation results obtained using ATENA show good agreement with the experimental data.

4. Validation of the finite element model

The frame beams were fabricated from C35 concrete, measuring 200 mm × 500 mm in section. Longitudinal reinforcement comprising HRB400 steel bars: 4C22 bars in two layers at the top and 6C22 bars in two layers at the bottom. Stirrups of HRB400 steel were spaced at C10@100/200. Frame columns were constructed using C35 concrete with a 400 mm × 400 mm cross-section, reinforced both longitudinally and transversely with HRB400 steel. The infill wall was cast in C35 concrete to a height of 3100 mm and contained a double-layer, bi-directional A3@100 reinforcement mesh. Table 2 presents the geometric and reinforcement parameters of the nine specimens, which were designed to evaluate the effects of the frame height-to-width ratio, wall thickness, and tie reinforcement arrangement on the structural performance of the frame-infill system.

Table 2 Specimen design table (unit: mm)

Specimen number	Factor	Wall width	Aspect	Wall thickness	Wall-beam tie-bars	Wall-column tie bars
K1	comparison	5600	0.55	100	C16@1200	C16@600
K2	Wall aspect ratio	6600	0.47	100	C16@1200	C16@600
K3		4600	0.67	100	C16@1200	C16@600
K4	Wall thickness	5600	0.55	150	C16@1200	C16@600
K5		5600	0.55	200	C16@1200	C16@600
K6	Wall-column tie bars	5600	0.55	100	C16@1200	C16@450
K7		5600	0.55	100	C16@1200	C16@750
K8	Wall-beam tie-bars	5600	0.55	100	C16@600	C16@600
K9		5600	0.55	100	C16@1800	C16@600

5. Finite element model analysis results

Finite element analysis was performed after the precast infill wall had fully cured. The wall was subsequently used as side formwork for casting the adjacent frame columns, employing a secondary casting procedure similar to Moretti's method. Given that the structural system incorporated cast-in-place concrete columns and composite beams, the elastic modulus at the wall-column interface was assigned 3.15×10^4 N/mm² in the FE model.

At the wall-beam interface, the presence of a C20-grade fine aggregate concrete layer was modeled with an elastic modulus of 2.55×10^4 N/mm², with the shear modulus set to 40% of this value. This modeling approach maintains a consistent representation of interface stiffness and contact behavior relative to actual construction details.

The three-level sweeps in aspect ratio, wall thickness, and tie densities can be interpreted as a deterministic local sensitivity study with respect to key design parameters, revealing monotonic and physically consistent trends without invoking full probabilistic sampling. These parameters were selected based on both prior literature and practical design relevance.

Aspect ratio and wall thickness are identified in design codes and seismic guidelines as first-order factors governing infill stiffness and load transfer, while tie reinforcement is a critical connection detail highlighted in experimental studies. Other factors, such as concrete strength, reinforcement ratio, and boundary frame stiffness, were deliberately held constant at representative values to isolate the effects of geometry and tie detailing.

This controlled approach follows common practice in parametric finite element studies and avoids confounding interactions. Future studies may extend the framework to systematically vary those additional parameters. Experimental studies demonstrate that frame-infill wall systems retain deformation capacity even after reaching peak loads. Ultimate displacement is conventionally defined as the displacement corresponding to 85% of the maximum load $P_{\max}$ on the descending branch of the load-displacement curve. This definition aligns with the Regulations on Seismic Test Methods for Buildings (JGJ101-96) [22], which mandate loading specimens beyond the peak load until the residual load drops to 0.85 times the peak load. Consistent with this standard, the ultimate displacement in this study is defined as the displacement at 0.85 $P_{\max}$ on the post-peak portion of the curve.

The ductility factor is defined as the ratio of the ultimate displacement, Δ_u, to the yield displacement, Δ_y, of the structural system.

$$\mu = \frac{\Delta_u}{\Delta_y} \tag{8}$$

However, for structural members that do not exhibit a clear yield point, this factor cannot be determined directly. In this study, the yield displacement is defined using the equivalent elasto-plastic system method [23], where it is taken as the displacement corresponding to the intersection of the load-displacement curve with a secant stiffness line drawn at 75% of the peak load. This method is illustrated in Fig. 8, which shows how the yield point is identified on the curve.

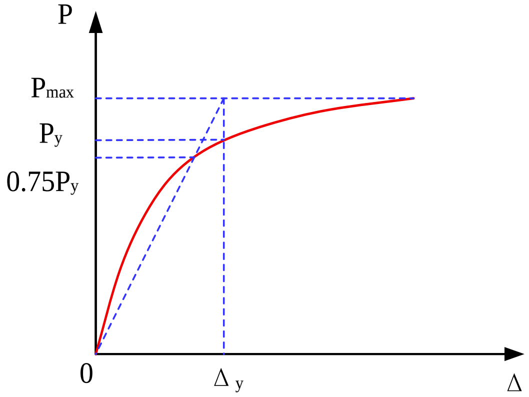

Fig. 8 Schematic diagram for determining the yield load (yield point) of the structure

5.1. Influence of height-to-width ratio on frame–infill wall performance

The height-to-width ratio (aspect ratio) of an infill wall is widely recognized as a key parameter affecting the lateral stiffness and overall mechanical performance of frame structures. The stiffness of the frame-infill wall system arises from the combined action of the infill panel and the surrounding frame, and a change in the infill wall's aspect ratio can significantly alter this stiffness balance. In this study, three aspect ratios of the precast infill wall (0.47, 0.55, and 0.67, height/width) are analyzed. Fig. 9 shows the load-displacement curves for specimens K1, K2, and K3 representing these aspect ratios. Likewise, Fig. 10 depicts the crack patterns observed at specific displacement levels for each case: (a) 10.1 mm for K1, (b) 9.9 mm for K2, and (c) 11.0 mm for K3. Key performance metrics, including peak load, yield point, and ductility for the different aspect ratios, are compared in Table 3.

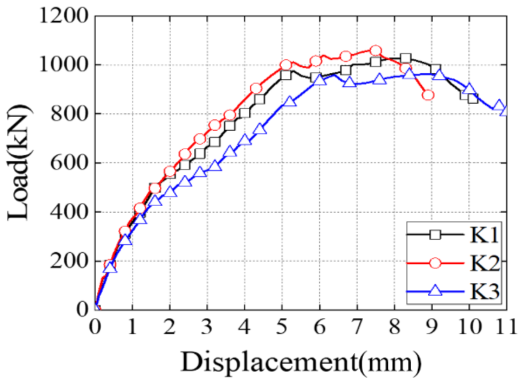

Fig. 9 Comparison of load-displacement curves of K1, K2, and K3 specimens

(a) Specimen K1

(b) Specimen K2

(c) Specimen K3

Fig. 10 Crack distribution in specimens with different wall aspect ratios at selected displacements

According to the results in Fig. 10 and Table 3, reducing the infill wall's height-to-width ratio results in a stiffer frame–wall system. A lower aspect ratio (i.e., a shorter, wider wall) increases the system's lateral stiffness, resulting in higher peak load and ultimate load capacities. However, this increase in stiffness comes at the expense of deformation capacity: as the wall's aspect ratio decreases, both the yield displacement and the displacement at peak load are reduced. This reduction in ductility can be attributed to the limited frame flexibility and reduced confinement effect provided by taller walls, which restricts energy dissipation capacity during lateral loading. Quantitatively, when the aspect ratio is changed from 0.47 (short wall) to 0.67 (taller wall), the peak displacement of the system decreases by approximately 9%, while the displacement at peak load (an indicator of initial stiffness) increases by approximately 17%. Among the cases studied, the infill wall with an intermediate aspect ratio of roughly 0.55 provides the best overall ductility, indicating a balanced trade-off between strength and deformability for this configuration.

To facilitate broader generalization, the peak load values have also been normalized by wall area, as shown in Table 3. Normalized results reveal consistent trends: lower aspect ratio walls carry higher load per unit area, though with reduced ductility.

Table 3 Comparison of load-carrying capacity and ductility of specimens with different aspect ratios

Specimen number	Yield load/kN	Yield displacement/mm	Peak load/kN	Peak displacement/mm	Ultimate load/kN	Ultimate displacement/mm	Ductility factor
K1	934.9	4.9	1028	8.3	861.7	10.1	2.06
K2	977.6	4.8	1058	7.5	876.4	9.9	1.85
K3	891.2	5.7	962.3	8.8	806.7	11	1.93

Furthermore, the crack patterns in Fig. 11 indicate that a lower height-to-width ratio causes more extensive cracking in the infill wall. Specimen K1 (the wall with the lowest aspect ratio) developed a greater number of cracks with longer crack lengths across the panel. Despite differences in the extent of cracking, all three specimens exhibited broadly similar trends in crack distribution. In each case, because the infill wall's reinforcement ratio was relatively low, significant tensile cracking occurred in the wall's tension zone. Flexural cracks were also observed at the base of the frame columns, along with concentrated cracking at the beam-column joints (frame nodes), where higher stresses arise during lateral loading. These observations suggest that while the aspect ratio alters the quantity and length of cracks, the general locations and modes of cracking (tensile cracking in the wall and flexural cracking in the frame) remain consistent.

5.2. *Influence of wall thickness on frame-infill wall performance*

The thickness of the infill wall is another crucial factor affecting the frame-wall system's behavior. In this section, wall thicknesses of 100 mm (baseline, specimen K1), 150 mm (specimen K4), and 200 mm (specimen K5) are compared, and their impact on structural performance is evaluated. Fig. 11 shows the load-displacement curves for these three wall thickness scenarios, while Fig. 12 illustrates the corresponding crack patterns observed at key displacement levels: (a) 7.7 mm for the 150 mm wall and (b) 8.2 mm for the 200 mm wall. Table 4 provides a side-by-side summary of the load-bearing capacity and ductility metrics for each wall thickness.

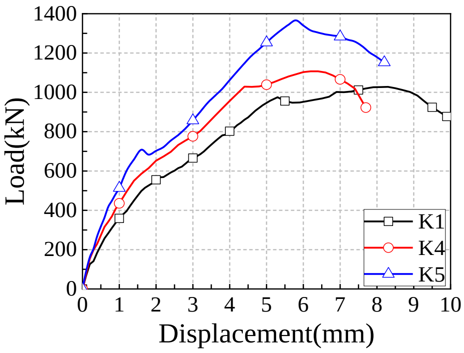

Fig. 11 Comparison of load-displacement curves of K1, K4, and K5

(a) Specimen K4 (b) Specimen K5

Fig. 12 Crack pattern comparison for different infill wall thicknesses

Increasing the wall thickness significantly enhances the stiffness and strength of the frame-infill system. As shown in Fig. 12 and quantified in Table 4, an increase in infill wall thickness results in higher peak load capacity and a delayed onset of yielding. For instance, increasing the wall thickness from 100 mm to 150 mm results in an approximate 8% increase in the structure's peak load, while increasing it to 200 mm results in approximately a 32% increase. These improvements indicate that a thicker wall can sustain significantly greater lateral loads before failure. Moreover, the yield point of the system, defined as the point at which the load-displacement curve begins to soften, occurs at a larger displacement for thicker walls, suggesting improved initial stiffness and load resistance.

Table 4 Comparison of load-carrying capacity and ductility of specimens with different aspect ratios

Specimen number	Yield load/kN	Yield displacement/mm	Peak load/kN	Peak displacement/mm	Ultimate load/kN	Ultimate displacement/mm	Ductility factor
K1	934.9	4.9	1028	8.3	861.7	10.1	2.06
K4	1028	4.5	1107	6.3	922.5	7.7	1.71
K5	1253	5.1	1366	5.8	1152	8.2	1.62

However, there are trade-offs associated with increasing wall thickness. While a thicker wall improves strength and stiffness, it tends to reduce the structure's ductility (i.e., its ability to undergo deformation without a significant loss in strength). For instance, specimen K5 (200 mm wall) showed signs of earlier cracking in the frame: a crack appeared at the base of the left frame column at a relatively small displacement of 2.6 mm, which subsequently limited the structure's load-bearing capacity beyond that point.

In general, as wall thickness increases, the infill wall itself develops fewer cracks and remains more intact, as shown in Fig. 12. Instead, larger gaps or separations tend to form at the interfaces with the frame (e.g., between the wall and columns), indicating that the frame is accommodating more deformation.

Notably, the overall crack distribution pattern in the frame-wall system remains relatively consistent across different wall thicknesses; all cases (100 mm, 150 mm, and 200 mm) exhibit similar crack locations. However, the density of cracks in the wall decreases with increasing thickness. Thicker walls exhibit more limited cracking within the panel and show a shift in deformation toward the frame elements, which is consistent with a reduction in system ductility as the infill wall becomes more rigid.

5.3. Effect of wall-column tie reinforcement on structural performance

In precast frame-infill systems, wall-column tie bars (vertical ties anchoring the infill wall to the adjacent columns) are crucial for ensuring composite action between the wall and the frame. This section examines how different wall-column tie reinforcement arrangements influence the structural behavior of the frame. Three configurations are analyzed: specimen K1 with a baseline tie spacing, specimen K6 with denser ties (closer spacing, higher reinforcement ratio), and specimen K7 with more widely spaced ties (lower reinforcement ratio). Fig. 13 shows the load-displacement curves for K1, K6, and K7, illustrating the effect of tie bar spacing on the overall structural stiffness and strength. Correspondingly, Fig. 14 compares the crack patterns for two extreme cases: (a) the dense tie configuration and (b) the sparse tie configuration. Key performance indicators, including peak load, yield displacement, and ductility, for each tie arrangement are summarized in Table 5.

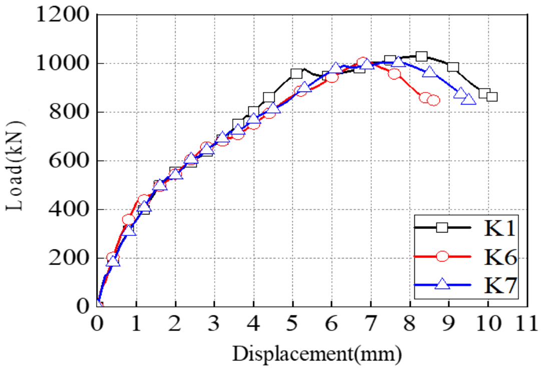

Fig. 13 Comparison of load-displacement curves of K1, K6, and K7

(a) Specimen K6 (b) Specimen K7

Fig. 14 Crack pattern comparison for wall–column tie configurations

Table 5 Comparison of load-carrying capacity and ductility of specimens with different infill wall thicknesses

Specimen number	Yield load/kN	Yield displacement/mm	Peak load/kN	Peak displacement/mm	Ultimate load/kN	Ultimate displacement/mm	Ductility factor
K1	934.9	4.9	1028	8.3	861.7	10.1	2.06
K6	887.8	5.3	1002	6.9	847.2	8.6	1.61
K7	1885.9	5.2	1004	7.3	846.5	9.5	1.83

The results in Fig. 13 and Table 5 indicate that the spacing of wall-column tie bars predominantly influences the deformation capacity of the structure, rather than its initial strength. When the wall-column ties are placed more closely (as in K6), the frame-wall system exhibits a delayed yield point and a reduction in ultimate deformation capacity, meaning it becomes less flexible but can sustain loads without yielding until a larger displacement occurs. Among the tested configurations, the intermediate tie spacing, as in the arrangement of specimen K1, provided a good balance. However, the specimen with the densest ties (K6, tie spacing 600 mm) achieved the highest peak load and exhibited an optimal level of ductility, thereby enhancing its seismic performance. In contrast, the specimen with the most widely spaced ties (K7) showed a slightly lower peak load and earlier onset of yielding.

Another notable finding is the effect of tie spacing on the post-peak (residual) load capacity. During extended loading into the post-peak regime (beyond $0.85P_{max}$), the configuration with dense ties (K6) retained a higher residual strength compared to the others. The residual load of K6 was approximately 18% higher than that of the baseline K1 and 25% higher than that of the wide-spacing specimen K7.

Although energy dissipation and hysteretic curves could provide a more detailed picture of post-peak behavior, the residual strength adopted here serves as a reliable indicator of structural integrity under cyclic demands. Future work may extend the present framework to include energy-based evaluation metrics.

These residual strength measurements suggest that closer wall-column tie spacing helps maintain structural integrity even after significant cracking and a reduction in peak load. Crack pattern observations, as shown in Fig. 14, support these findings: all specimens displayed similar crack distributions concentrated at column bases and tie points, with no adverse crack concentrations induced by tie spacing variations. Essentially, reducing the wall–column tie spacing enhances the post-damage load-carrying capacity without altering the crack localization patterns.

From a practical perspective, the investigated tie configurations are also consistent with typical construction practices, and both dense and sparse tie spacings fall within ranges that can be feasibly implemented in precast construction. This confirms that the numerical findings are not only of theoretical interest but also of engineering applicability.

5.4. Effect of wall-beam tie reinforcement on structural performance

Another essential connection detail in the frame-infill system is the wall-beam tie bar—a horizontal tie that connects the top of the infill wall to the frame’s beam. This section examines how variations in the wall-beam tie bar configuration affect the structural behavior of the system. Three scenarios are compared: specimen K1 with a standard arrangement of wall-beam ties, specimen K8 with an increased number of wall-beam tie bars (closer spacing or additional ties), and specimen K9 with a reduced number of wall-beam ties (wider spacing or omitted ties in some locations). Fig. 15 plots the load-displacement curves for K1, K8, and K9, highlighting differences in stiffness and strength due to the wall-beam tie arrangements. Meanwhile, Fig. 16 illustrates the crack patterns for two contrasting cases: (a) the configuration with extra (closely spaced) wall-beam ties, and (b) the configuration with fewer (widely spaced) wall-beam ties. Key outcomes, including peak load capacity and system ductility for each configuration, are summarized in Table 6.

The selected tie spacings (600 mm, 1200 mm, and 1800 mm) were chosen to represent typical construction practices, covering dense, standard, and sparse reinforcement intervals that are commonly adopted in precast concrete projects. This ensures that the investigated cases are not only theoretically distinct but also practically meaningful.

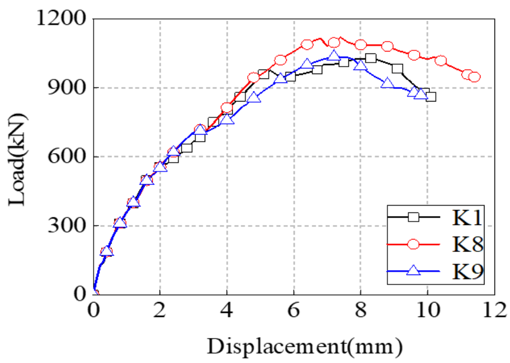

Fig. 15 Comparison of load-displacement curves of K1, K8, and K9

(a) Specimen K8 (b) Specimen K9

Fig. 16 Comparison of crack patterns for wall–beam tie configurations

Although a detailed narrative of the results for the wall-beam tie variations was not provided in earlier sections, the data from Fig. 15 and Table 6 suggest trends analogous to those observed for wall-column ties. In general, adding more wall-beam tie bars (as in K8) tends to slightly increase the frame-wall system's peak load capacity and stiffness, since the beam more effectively restrains the infill wall. Conversely, using fewer tie bars (as in K9) can lead to a minor reduction in peak load and a more flexible response. However, once the peak load is exceeded, the spacing of wall-beam ties appears to have a less pronounced effect on the post-peak behavior compared to wall–column ties. For instance, beyond $0.85P_{max}$, all three specimens (K1, K8, and K9) retain a comparable portion of their strength, indicating that the wall-beam tie configuration does not drastically change the residual load capacity.

Table 6 Comparison of load-carrying capacity and ductility of specimens with different wall-beam tie reinforcements

Specimen number	Wall–beam tie bar spacing /m	Yield load /kN	Yield displacement /mm	Peak load /kN	Peak displacement /mm	Ultimate load /kN	Ultimate displacement /mm	Ductility factor
K1	1200	934.9	4.9	1028	8.3	861.7	10.1	2.06
K8	600	1010	5.5	1119	7.4	974.3	11.4	2.09
K9	1800	935.8	5.6	1035	7.2	868.3	9.8	1.75

The crack pattern comparisons in Fig. 16 show that all configurations share a similar crack localization, with major cracks forming at the corners of the infill wall and along the interfaces with the frame (especially near the beam level). However, there are some differences in crack intensity. With an enhanced wall-beam tie arrangement, as shown in Fig. 16 (a), the infill wall remains more integrated with the beam, resulting in slightly fewer or narrower cracks at the top interface. In contrast, the specimen with reduced ties, as shown in Fig. 16 (b), exhibits a marginally wider separation between the wall and beam, manifesting as cracks or gaps. Despite these differences, the overall failure mode—diagonal compression cracking in the wall and flexural cracking in the frame—remains consistent.

In summary, a denser wall–beam tie configuration can marginally improve both strength and rigidity, enhancing the composite action between the infill wall and the frame. However, a considerable tie spacing (beyond approximately 1200 mm, as reflected in specimen K9) does not significantly reduce peak strength; instead, it primarily affects the degree of coupling between the wall and the beam without introducing new failure modes.

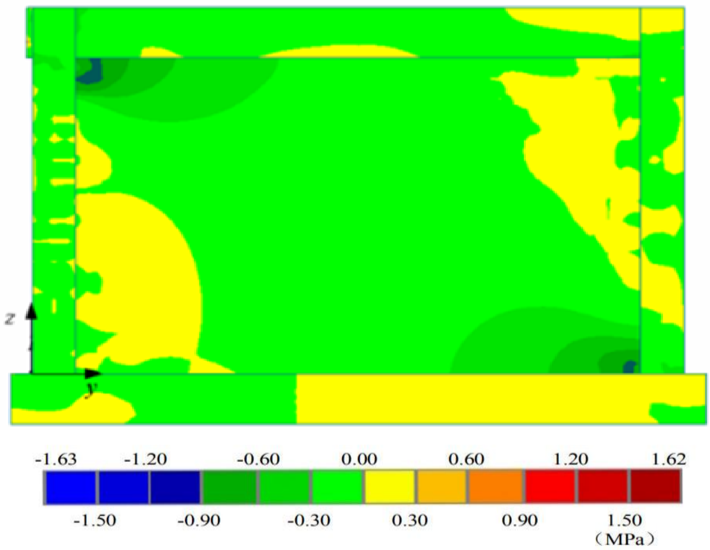

Fig. 17 Y-direction (vertical) stress distribution in specimen K1 at peak load

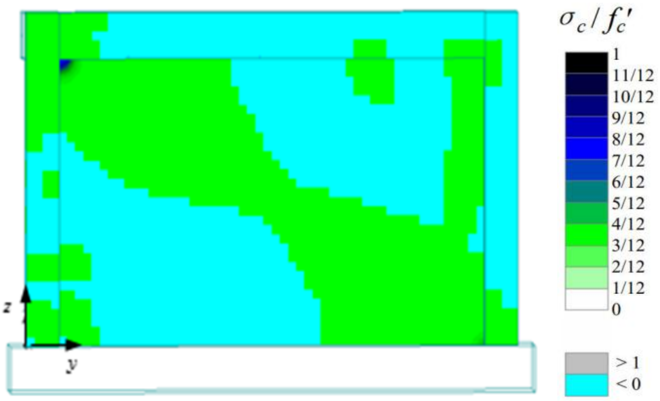

Fig. 18 Equivalent plastic strain distribution in specimen K1 at peak load

Across all the simulated models (K1 through K9), the crack distribution maps reveal that while the various parameters (aspect ratio, wall thickness, and tie configurations) alter the severity or density of cracking, the fundamental pattern of cracks remains consistent. In every case, the infill wall develops significant tensile cracks, especially in the wall's right-side tensile zone under lateral loading, with additional cracks appearing in the left-side tensile region. The frame columns consistently show flexural cracking, with the left-side column (facing the direction of applied load) usually experiencing more pronounced crack formation than the right-side column. These similarities suggest that the overall failure mode, characterized by diagonal tension cracks in the infill and flexural yielding of frame members, remains qualitatively unchanged despite variations in design parameters, even though the exact load at which cracks form and their dispersion can differ.

The force transfer mechanism in the frame–infill wall system is clearly illustrated by the behavior of specimen K1 at peak load. As described by the Y-direction stress field in Fig. 17 and the equivalent plastic strain contour in Fig. 18, the infill wall and frame act together to channel forces diagonally through the wall. Specifically, the horizontal (lateral) force applied at the top left of the frame travels down to the bottom right of the frame, mainly through the infill wall. The distribution of the equivalent plastic strains follows a similar diagonal path from the loaded corner to the opposite support. This stress and strain pattern confirms that the infill wall functions as an equivalent diagonal compression strut within the frame—a behavior well-documented in infill wall research. In other words, under lateral load, the infill panel carries compression along a diagonal, taking on a truss-like role that braces the frame. This finding is consistent with literature results [20], reinforcing the validity of the finite element models' representation of the frame–wall interaction.

6. Conclusions

This study performed nonlinear finite element analyses, validated with experimental benchmarks, to evaluate the effects of key design parameters on the mechanical behavior of precast concrete infill wall systems. The primary findings are:

(1) Decreasing the infill wall height-to-width aspect ratio notably improves lateral stiffness, peak load, and ultimate capacity while reducing deformation capacity. An aspect ratio of around 0.55 provides an optimal balance between stiffness and ductility.

(2) Increasing the thickness of infill walls significantly enhances structural stiffness, delays yielding, and raises peak load capacity. However, thicker walls shift damage to frame elements, thus reducing overall structural ductility.

(3) Increasing the density of wall-to-column tie reinforcement delays yielding and enhances initial stiffness and residual load capacity after peak loading, though slightly compromising ductility.

(4) Enhancing wall-to-beam tie reinforcement density moderately improves peak load capacity and stiffness, but wider spacing (exceeding approximately 1200 mm) reduces structural ductility without significantly affecting peak load.

(5) Numerical analyses of stress distributions and crack patterns validate that precast infill walls effectively function as diagonal compression struts under lateral loading, affirming the accuracy and reliability of the finite element modelling approach.

Nevertheless, this study has certain limitations. The boundary conditions were idealized, steel reinforcement was modelled as linear-elastic–perfectly plastic without considering bond–slip effects, and no formal uncertainty quantification was carried out. These assumptions may influence the generalization of the results. Future research could address these limitations by incorporating more realistic boundary conditions, nonlinear bond–slip models, and probabilistic approaches for uncertainty assessment. In addition, optimization-based parametric studies and experimental–numerical hybrid investigations would further enhance the applicability of precast infill wall design in engineering practice.

Conflicts of Interest

The authors declare no conflict of interest.

References

[1] A. Pavese and D. A. Bournas, "Experimental Assessment of the Seismic Performance of a Prefabricated Concrete Structural Wall System," Engineering Structures, vol. 33, no. 6, pp. 2049-2062, 2011.
[2] Q. Gu, G. Dong, X. Wang, H. Jiang, and S. Peng, "Research on Pseudo-Static Cyclic Tests of Precast Concrete Shear Walls with Vertical Rebar Lapping in Grout-Filled Constrained Hole," Engineering Structures, vol. 189, pp. 396-410, 2019.
[3] L. Dang, S. Liang, X. Zhu, M. Zhang, and Y. Song, "Seismic Performance of Precast Concrete Wall with Vertical Energy-Dissipating Connection," The Structural Design of Tall and Special Buildings, vol. 30, no. 2, article no. e1820, 2021.
[4] G. Xu, T. Guo, and A. Li, "Self-Centering Rotational Joints for Seismic Resilient Steel Moment Resisting Frame," Journal of Structural Engineering, vol. 149, no. 2, article no. 04022245, 2023.
[5] G. Xu, T. Guo, A. Li, and H. Zhang, "Self-Centering Beam-Column Joints with Variable Stiffness for Steel Moment Resisting Frame," Engineering Structures, vol. 278, article no. 115526, 2023.
[6] A. Fiore, A. Netti, and P. Monaco, "The Influence of Masonry Infill on the Seismic Behaviour of RC Frame Buildings," Engineering Structures, vol. 44, pp. 133-145, 2012.
[7] F. Xiong, Y. Wang, Z. Wang, and Y. Liu, "Seismic Performance of Coupled Precast Concrete Wall Panels Connected by Novel Vertical Bolted Joints," Structures, vol. 70, article no. 107654, 2024.
[8] Y. C. Tang, H. N. Li, and C. Li, "Parametric Studies on Seismic Performance of New Precast Braced Concrete Shear Walls Under Cyclic Loading," Journal of Structural Engineering, vol. 149, no. 6, article no. 04023061, 2023.
[9] Y. Wang, F. Xiong, and Y. Liu, "Shaking Table Test of a Full-Scale Lightweight Bolt-Connected Concrete Sandwich Wall Panel Structure: Configuration Modification and Parametric Analyses," Journal of Structural Engineering, vol. 151, no. 9, article no. 04025138, 2025.
[10] B. Wu, F. L. Zhang, M. Zhang, and Y. Li, "Cyclic Loading Experiments on Seismic Performance of Precast Concrete Superposed Shear Walls with CFST End Columns," Journal of Building Engineering, vol. 96, article no. 110527, 2024.
[11] Q. Ge, Y. Meng, J. Ai, W. Zuo, F. Xiong, Y. Liu, and N. Dong, "Seismic Performance of Precast Concrete Sandwich Walls with Bolt-Steel Plate Connection," Engineering Structures, vol. 303, article no. 117402, 2024.
[12] F. Chen, Z. Yu, Y. Yu, Z. Li, S. Cheng, G. Zhang, and C. Cui, "Experimental Investigation of Seismic Performance of Precast Concrete Shear Walls with Overlapping U-Bar Loop Connections," Scientific Reports, vol. 14, article no. 26240, 2024.
[13] M. Sun, S. Zhang, J. Yang, Y. Fang, and X. Xu, "Investigation on Seismic Behavior of a Novel Precast Shear Wall System with Different Infill Wall Constructions," Materials, vol. 16, no.23, article no. 7343, 2023.
[14] Y. Liu, W. Zhou, and X. Xie, "Experimental Study of Precast Self-Centering Concrete Shear Walls With External Friction Dampers," Journal of Building Engineering, vol. 68, article no. 106182, 2023.
[15] Q. Zheng, S. Chen, and W. Lin, "Numerical Study on Seismic Performance of a New Prefabricated Reinforced Concrete Structural System Integrated with Recoverable Energy-Dissipating RC Walls," Buildings, vol. 14, no.10, article no. 3243, 2024.

[16] S. Li, H. Liu, H. Wang, A. Zar, and C. Zhai, "Experimental Research on the Seismic Performance of Self-Centering Precast Concrete Frames with Infill Walls," Earthquake Engineering & Structural Dynamics, vol. 54, no. 9, pp. 2303-2324, 2025.

[17] D. A. Hordijk, "Local Approach to Fatigue of Concrete," Ph.D. dissertation, Department of Civil Engineering and Geosciences, Delft University of Technology, Delft, the Netherlands, 1991.

[18] Comité Euro-International du Béton, CEB-FIP Model Code 1990, Bulletin d'Information Nos. 213-214, Thomas Telford Services Ltd, London, 1993.

[19] J. G. M. van Mier, "Multiaxial Strain-Softening of Concrete, Part 1: Fracture," Materials and Structures, vol. 19, no. 111, pp. 179-190, 1986.

[20] H. C. Biscaia, C. Chastre, and M. A. G. Silva, "Modelling GFRP-to-Concrete Joints with Interface Finite Elements With Rupture Based on the Mohr-Coulomb Criterion," Construction and Building Materials, vol. 47, pp. 261-273, 2013.

[21] M. L. Moretti, T. Papatheocharis, and P. C. Perdikaris, "Design of Reinforced Concrete Infilled Frames," Journal of Structural Engineering, vol. 140, no. 9, article no. 04014062, 2014.

[22] China Academy of Building Sciences, Code of Test Methods for Building Seismic Resistance (JGJ 101-96), China Building Industry Press, Beijing, 1997.

[23] R. Park, "Evaluation of Ductility of Structures and Structural Assemblages from Laboratory Testing," Bulletin of the New Zealand Society for Earthquake Engineering, vol. 22, no. 3, pp. 155-166, 1989.